The Journal of Neuroscience
September 1986, 6(9): 2747-2756

Regional Distribution of Flunitrazepam Binding Constants: Visualizing K_d and B_{max} by Digital Image Analysis

Arthur W. Toga, Emily M. Santori, and Mariam Samaie

The Laboratory of Neuro Imaging, Department of Neurology and Neurological Surgery, and The McDonnell Center for the Study of Higher Brain Functions, Washington University School of Medicine, St. Louis, Missouri 63110

We demonstrate direct visualization of benzodiazepine binding parameters collected in a ^{3}H-flunitrazepam saturation study. In this way the relationship between anatomy and specific binding, K_d and B_{max}, can be appreciated. These experiments have resulted in image representations of specific flunitrazepam binding, K_d and B_{max}. The images retain the anatomic localization inherent in the original autoradiogram and hence make these parameters amenable to visual survey. Binding constants were consistent with data presented elsewhere in the literature. The image of B_{max} showed regional heterogeneity. K_d on the other hand, was relatively homogeneous. These results demonstrate a means by which autoradiographic binding experiments can be extended to saturation studies without significant loss of data.

Techniques used to measure and analyze receptor densities have become increasingly sophisticated. Early experiments demonstrated that the binding of radioactive ligands to membrane preparations could be used to study biological receptors (Cuatrecasas, 1974). Benzodiazepine receptors were among the first receptors characterized in this way (Bosmann et al., 1977; Mohler and Okada, 1977; Squires and Braestrup, 1977). More recently, ligand binding techniques have been applied to whole-tissue sections. This advance has allowed for light-microscopic examination of benzodiazepine receptor densities in discrete regions (Unnerstall et al., 1981; Young and Kuhar, 1979, 1980). By coexposing radioactive standards and using spot densitometric techniques, quantitative benzodiazepine receptor densities and affinities have been calculated (Palacios et al., 1981; Unnerstall et al., 1982).

Digital imaging technologies are just beginning to be applied to the analysis of quantitative autoradiographic receptor binding data. One of the first applications has been color coding of monochrome autoradiograms to enhance subtle variations (Goochee et al., 1980). In addition, the ease with which mathematical transformations of digital images can be performed has greatly facilitated the quantification of autoradiographic images. One difficulty that still remains is that meaningful binding results such as specific binding and the kinetic parameters B_{max} and K_d still require discrete measurements of several sections. In making these calculations the ability to illustrate the relationship between receptor binding and histology is lost.

Received Jan. 7, 1986; accepted Feb. 24, 1986.

This work was supported by funds from The Whitaker Foundation and research grants from the NIH, National Institutes of Neurological and Communicative Disorders and Stroke (NS14834), National Institute of Aging (AG05681), and Division of Research Resources (RRG1380). We wish to thank Ms. Tamara Arnicar and Mr. George Kossl for their invaluable assistance.

Correspondence should be addressed to Arthur W. Toga, The Laboratory of Neuro Imaging, Department of Neurology and Neurological Surgery, Washington University School of Medicine, 660 South Euclid Avenue, St. Louis, MO 63110.

In this paper we present a series of procedures that provide a direct visualization of basic benzodiazepine binding parameters obtained in a ^{3}H-flunitrazepam saturation study. Our intent was to preserve the anatomic (spatial) relationships of specific binding and B_{max} and K_d results obtained from an Eadie-Hofstee analysis of the saturation data.

We divided the problems into 4 steps: (1) aligning the autoradiograms, (2) averaging representative sections and generating specific binding images, (3) performing a linear regression on image data from increasing concentrations, and (4) transforming the images and displaying the y-intercept (B_{max}) and slope (K_d).

Preliminary results from this work were presented at the 1985 annual meeting of the Society for Neuroscience (Toga et al., 1985).

Materials and Methods

Tissue preparation for image alignment

The arithmetic operations performed on the image data to obtain specific binding, K_d and B_{max}, must be performed on aligned sections. We developed a method of aligning the images using fiducial marks. In preparing the rat brain for sectioning, 2 brain paste-filled fiducial columns of PE 205 tubing were freeze-mounted along with the brain onto an object holder. The blocking apparatus shown in Figure 1*A* was used to fix the orientation of the brain and set the fiducial columns straight and orthogonal to the object holder. The brain and 2 pieces of tubing were embedded in a gelatin matrix (4.5 g/ml; 300 bloom) and frozen in liquid freon-12. This particular gelatin formulation allowed the least migration of fiducial marks as the sections were cut. As shown in Figure 1, *B, C,* each section contained the brain tissue and 2 slices of the fiducial column (brain paste). Following the binding procedures, both the brain section and the fiducial marks became radioactive and thus autoradiographically detectable. The PE tubing kept the spots circular so the fiducial marks were well circumscribed. Since the spots were positioned outside the brain tissue, they did not interfere with the image. Alignment is achieved by digitally moving (translating and rotating) one image relative to another until the fiducial marks are aligned. The programs that performed these operations are described below.

Binding

A modified version of the autoradiographic methods described by Young and Kuhar (1979) was used. Briefly, 10 μm coronal sections of rat brain plus fiducials were cut on a cryostat and thaw-mounted onto subbed coverslips. The samples were dried in an ice-cold desiccator under vacuum pressure for 2–3 hr. Sections were stored overnight at −60°C prior to binding.

Coverslips with mounted tissue sections were incubated with tritiated flunitrazepam (FLU, 84.3 Ci/mmol; New England Nuclear Corp.) in 170 mM Tris-HCl (pH 7.4) for 90 min on ice. Triplicate sections were incubated at 1 of 5 ligand concentrations ranging from 0.40 to 9.83 nM. Nonspecific binding (NSp) at the 2 highest FLU concentrations was determined in the presence of 1 μM clonazepam (Hoffman La Roche). The sections received a 2 min rinse with ice-cold buffer, followed by rapid freezing on dry ice. Room air was used to blow off excess rinse

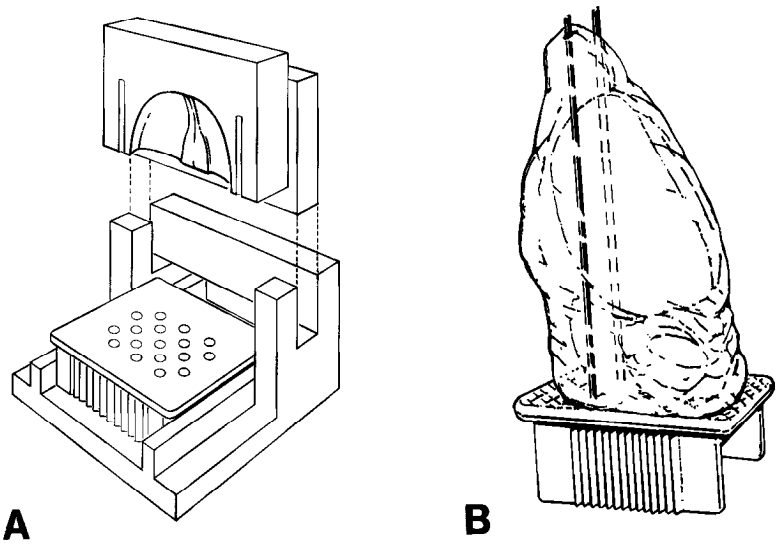

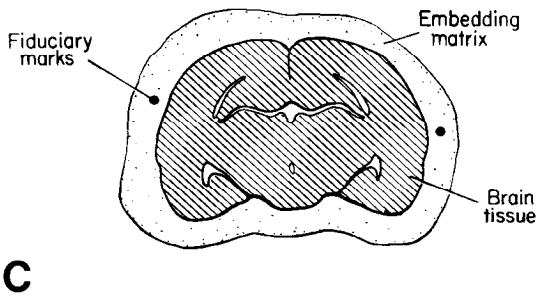

Figure 1. *A,* Blocking apparatus used to fix the orientation of the brain and 2 brain paste-filled fiducial columns of PE 205 tubing orthogonal to the object holder. *B,* The brain and 2 pieces of tubing were embedded in a gelatin matrix and frozen in liquid freon. *C,* Frozen sections, 10 μm, were cut and thaw-mounted onto subbed coverslips. The sectioned fiducial column produced marks that were fixed relative to the brain tissue and easily detectable using digital imaging techniques.

and to dry the sections. Dried sections were coexposed with tissue calibrated (^{3}H) plastic standards to LKB Ultrofilm. This permitted accurate conversion between optical density units and concentration of radioactivity (Geary et al., 1985; Lysz et al., 1982).

Image Analysis

We developed a series of computer programs that automatically aligned the sections, based on the fiducial marks, subtracted NSp from total bonding, and performed the Eadie-Hofstee analysis. These were developed and executed on the computer system described below.

Equipment

Our image analysis system consists essentially of 3 interrelated components—an Eikonix model 785 flatbed digitizing scanner, a Gould/DeAnza IP8400 image processor, and a DEC VAX 11/750 computer. A printer/plotter, tape drive, Dunn model 632 color camera system, 1 GB disk storage, terminals, and monitors are also part of the system. Input (or locator) devices include a joystick and Summagraphics Bitpad. The field of view range of the digitizing scanner is approximately 18 cm to 5 mm square. A line of 2048 photodiodes moves through 2048 steps over 50 sec, giving 2048 × 2048 pixels, each having one of 4096 gray scale values. These values can then be converted to optical density units, concentrations of radioactivity, or other quantitative measures. A more complete description of this system is described in Toga et al. (1984). An illustration of the architecture is presented in Figure 3.

Alignment and averaging

The algorithms were developed using FORTRAN and PASCAL programming languages. The first step was to align triplicate sections so that they could be averaged prior to computing specific binding. The alignment algorithm is best described in flow chart form and is shown in Figure 2. Simply stated, the fiducial marks of the first image are designated the reference, and subsequent images are moved up or down, left or right until their left fiducial mark overlaps the left fiducial mark from the reference image. Then the image is rotated about the left fiducial mark until the right one is also aligned. Since the fiducial marks were cut from columns fixed relative to the tissue itself, when the fiducial marks are aligned, so is the tissue.

The triplicate sections were then averaged to give a "representative," rather than mean, image. The algorithm examines the density value for each of the image's picture elements (pixel). If 1 of the pixels deviated by more than 10% from the other 2, presumably due to a dust particle or scratch on the autoradiogram, it was discarded.

Specific binding

NSp binding was subtracted from the total binding representative images to obtain specific binding images. NSp binding at the 4 lowest FLU concentrations was approximated by multiplying the NSp image obtained at the highest FLU concentration by the ratios of the free concentrations (lower/max). This approximation was based on the prior observation that there was a linear relationship between the free FLU and NSp binding.

The total images were aligned to their corresponding NSp image, and each pixel from the NSp image was subtracted from the total image. If the result was a negative number, that pixel was assigned a value equivalent to background density. During these arithmetic operations, the image data were in the form of radioactivity. A fitted polynomial curve relating optical densities to known radioactive concentrations of tissue calibrated tritium standards was used to quantify the image data. The final data transformation converted the tissue concentrations from nCi/mg to fmol FLU/mg by dividing the radioactivity values by the ligand specific activity.

Since all of the total images were aligned to a single NSp image (or a mathematical derivative of the NSp image), all of the total images were aligned with one another. Thus, the resultant specific binding images were in alignment.

Eadie-Hofstee analysis

In order to carry out an Eadie-Hofstee analysis, a second series of digital images representing the bound/free variable was generated. Each specific image was divided by its corresponding free FLU concentration. Then for each picture element (pixel), a linear regression relating the bound/free and the bound values of the 5 FLU concentrations was performed. The slope of the regression yielded K_d and the y-intercept yielded B_{max}. Only after a total of 266,144 regressions (the total number of pixels in an image) had been performed could the images of B_{max} and K_d be presented.

The numeric values resulting from the arithmetic operations described above were fractional and of a scale that was not appropriate for visual presentation on a video color monitor. The range of data for K_d images was 2–3 orders of magnitude smaller than B_{max} or specific binding images. Therefore, for each kind of image, the values were transformed to optical density, then radioactive concentration. Finally they were scaled and pseudo-colored to better illustrate the variations in binding statistics.

Results and Discussion

Alignment

A prerequisite to any arithmetic operation on multiple images is that all the images must be aligned. The results of our fiducial approach to image alignment are shown in Figure 4. The artificially introduced (prior to sectioning the brain) fiducial marks were placed outside the perimeter of the brain so that they did not interfere with subsequent image analysis. In calculating specific binding and the other binding constants (K_d and B_{max}), the accuracy of the alignment is crucial because any errors introduced early on will be magnified by the repetitive nature of the image calculations. Although errors in the alignment are minimal using this approach, they can occur. In our procedure we attempted to reduce this error by averaging 3 sections to derive a "representative" coronal section. We feel that a representative coronal section is superior to a "mean" section because the mean could be heavily influenced by scratches or other imperfections in the film itself.

The algorithms developed to perform this operation were designed with the assumption that the sections themselves were coplanar, and hence only translational (movements in the x or y direction) and rotational corrections were made. The mechanics of serial sectioning on a freezing microtome make this assumption reasonable. A more detailed description of the algorithms is presented elsewhere (Toga and Arnicar, 1985).

Nonspecific binding

The NSp image obtained at the highest ligand concentration (9.83 nM) is shown in Figure 5. In previous experiments it was found that there was a linear relationship between the free ^{3}H-FLU concentration and NSp binding in whole sections. With this as an assumption, the NSp images at the 4 lower ligand concentrations were approximated from the 9.83 nM NSp image as described in Materials and Methods. The validity of this approach can be seen by comparing the regional NSp binding determined experimentally at the second highest ligand concentration (4.43 nM) with values that were approximated by multiplying each pixel in the 9.83 nM NSp image by the ratio of the concentrations (4.43/9.83). Real NSp binding for gray matter averaged 11 fmol/mg tissue, and the extrapolated estimated binding was 8 fmol/mg tissue.

Not all the binding contained in the 9.83 nM NSp binding image is true NSp binding. The dense binding apparent within the ventricular spaces is probably specific binding to the peripheral type benzodiazepine receptors. In tissues outside of the CNS, benzodiazepine receptors have been found that differ in affinity and ligand specificity from benzodiazepine receptors characterized within the brain (Braestrup and Squires, 1977; Mohler and Okada, 1977). Richards et al. (1981) have shown

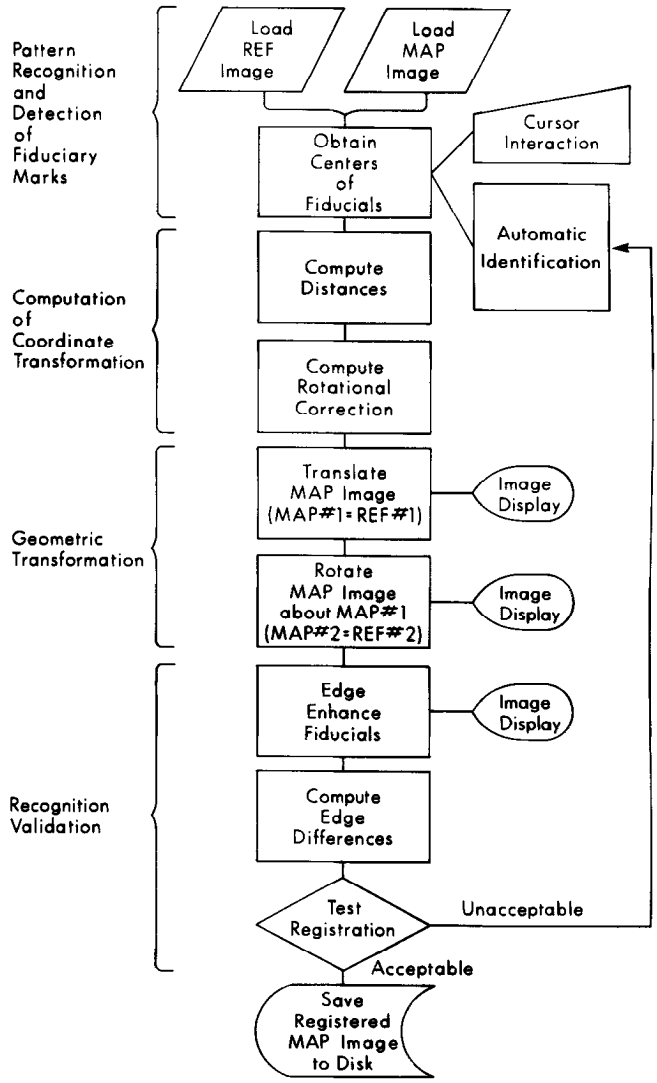

Figure 2. Flow chart of the algorithm used to align brain sections based upon fiducial marks. One section is moved relative to another until the marks and tissue are aligned. Note that only translational and rotational corrections were performed. Brain sections were assumed to be coplanar because of the mechanics of the freezing microtome.

that there is a high density of this peripheral type receptor in the ependymal lining of the ventricles and within the choroid plexus. These investigators also have shown that while FLU readily binds to this receptor, clonazepam has no affinity. Thus, the dense binding apparent within the ventricular spaces is probably specific FLU binding to the peripheral type benzodiazepine receptors on the choroid plexus and ependymal tissue that is not displaceable by clonazepam. In the ventricular region the method used to approximate NSp binding at the lower ligand concentrations is inaccurate, since the assumption of a linear relationship between ligand concentration and binding would be invalid.

Specific binding

The specific binding images produced following total minus NSp image subtractions are shown in Figure 6. These subtractions had to be performed on data in the form of concentrations of radioactivity because the 2 sets of autoradiograms, NSps, and totals were created using slightly different protocols. In order to detect the NSp binding of FLU, the tissue was exposed against

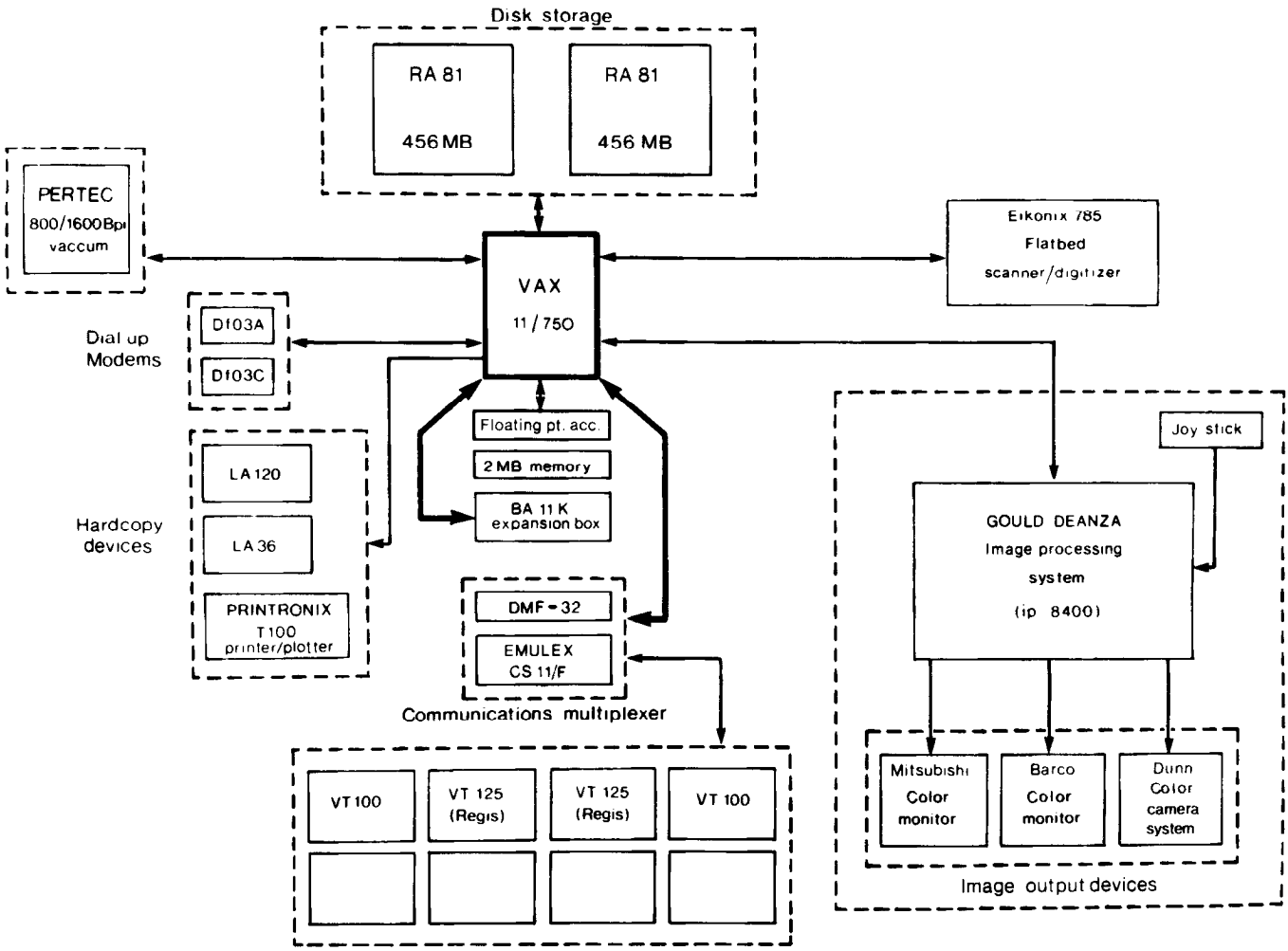

Figure 3. The major components of the imaging equipment. *Heavier lines* represent those components that are an integral part of the computer. The image processor is interfaced with the VAX using direct memory access and drives the color monitors and Dunn color camera system.

the film longer than total binding tissue. Since the relationship between optical density and concentration of radioactivity is nonlinear (Geary et al., 1985; Lysz et al., 1982), and arithmetic operations must be performed on equivalent sets of data, the images had to be converted to concentrations of radioactivity.

Comparison of the total image and the specific image (see Figs. 5, 6) reveals minor differences. This is because of the extremely low background NSp activity for this assay. Even at the highest ligand concentration, NSp binding rarely exceeded 10–15% of the specific binding. Nevertheless, the utility of calculating specific binding is apparent. For assays with higher backgrounds, an image subtraction technique will facilitate the detection of small changes in specific binding. For example, if there was a 20% change in specific binding, and NSp binding contributed 30% of the total radioactivity, then only 14% of the change would be apparent in the total binding autoradiogram.

Table 1. Hypothetical example of binding differences measured in total binding images versus specific binding images

	Hypothetical binding		% Change: stimulated vs control
	Control	Stimulated	
Specific	70	84	20
Nonspecific	30	30	—
Total	100	114	14

Asymmetries, for example, could be significantly different when measured as specific binding, while total binding measurements are not significantly different.

Binding constants

The saturation curve and Eadie-Hofstee plot for 1 region of cortex analyzed by standard spot densitometry is shown in Figure 7. These plots indicate saturable binding to an apparent single population of binding sites. Increasing evidence suggests that there are 2 types of central benzodiazepine receptors (Skolnick and Paul, 1982; Young et al., 1981). The apparent single class of sites labeled by FLU in this and other studies (Bosmann et al., 1977; Braestrup and Squires, 1978; Mohler and Okada, 1977; Squires and Braestrup, 1977) results from FLU binding to both sites with equal affinity.

The results of the pixel-by-pixel Eadie-Hofstee analysis of the saturation data are presented in Figures 8 and 9. The image of B_{max} (Fig. 8) is composed of the y-intercept values of the linear regression of Bound versus Bound/Free. It is essentially a more concentrated version of the specific image generated at the highest ligand concentration. In the cortex, the B_{max} pixel values average 207.4 fmol/mg tissue. This is consistent with the B_{max} of 205.5 fmol/mg tissue found by spot densitometry (Fig. 7). Following a units conversion from mg tissue to mg protein,

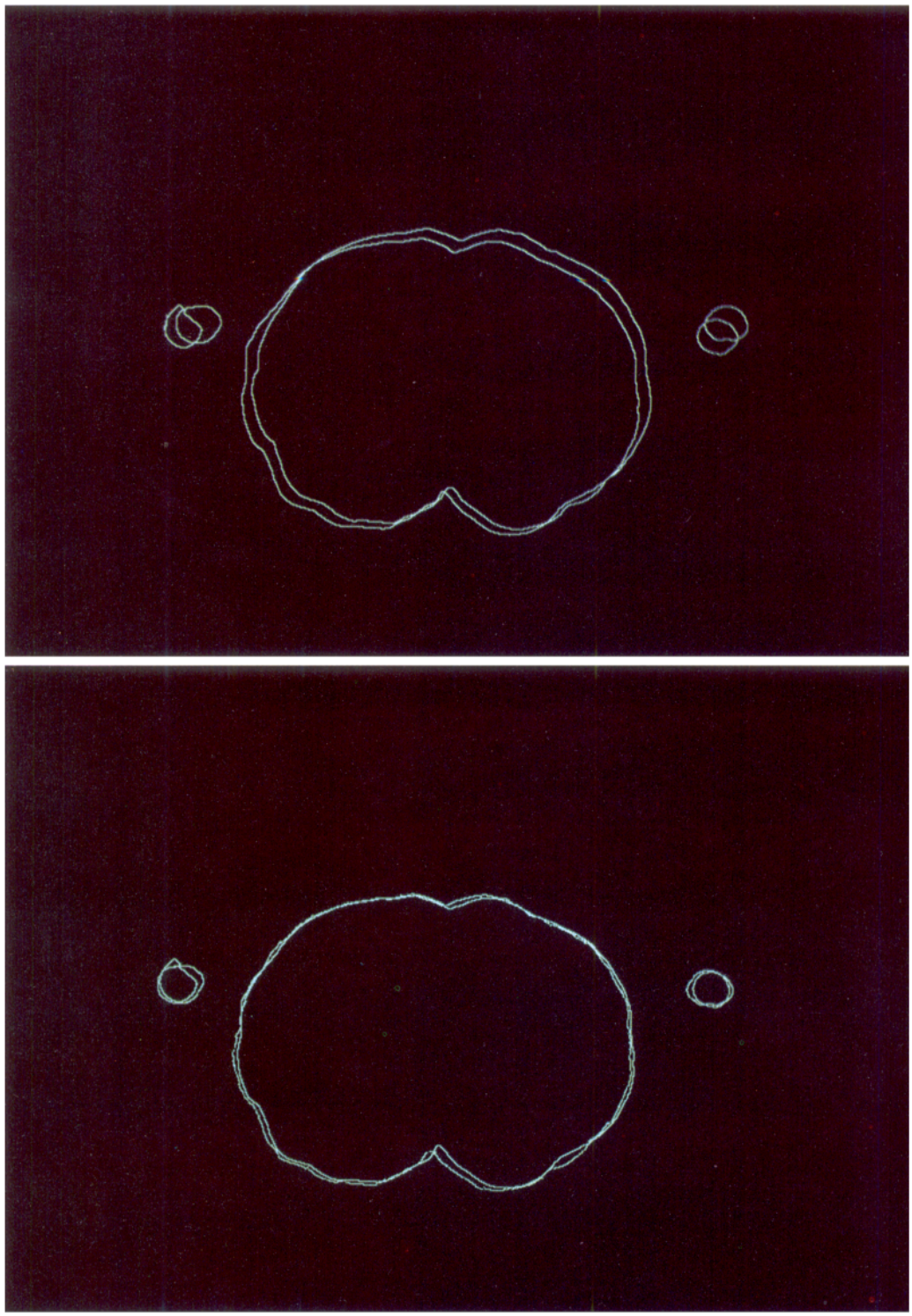

Figure 4. Contours shown were generated using edge-detection algorithms to illustrate the outlines of a coronal section and its accompanying fiducial marks. *Top,* Two images are shown, one overlapping the other. These images have not yet been aligned. *Bottom,* Results of the alignment procedure.

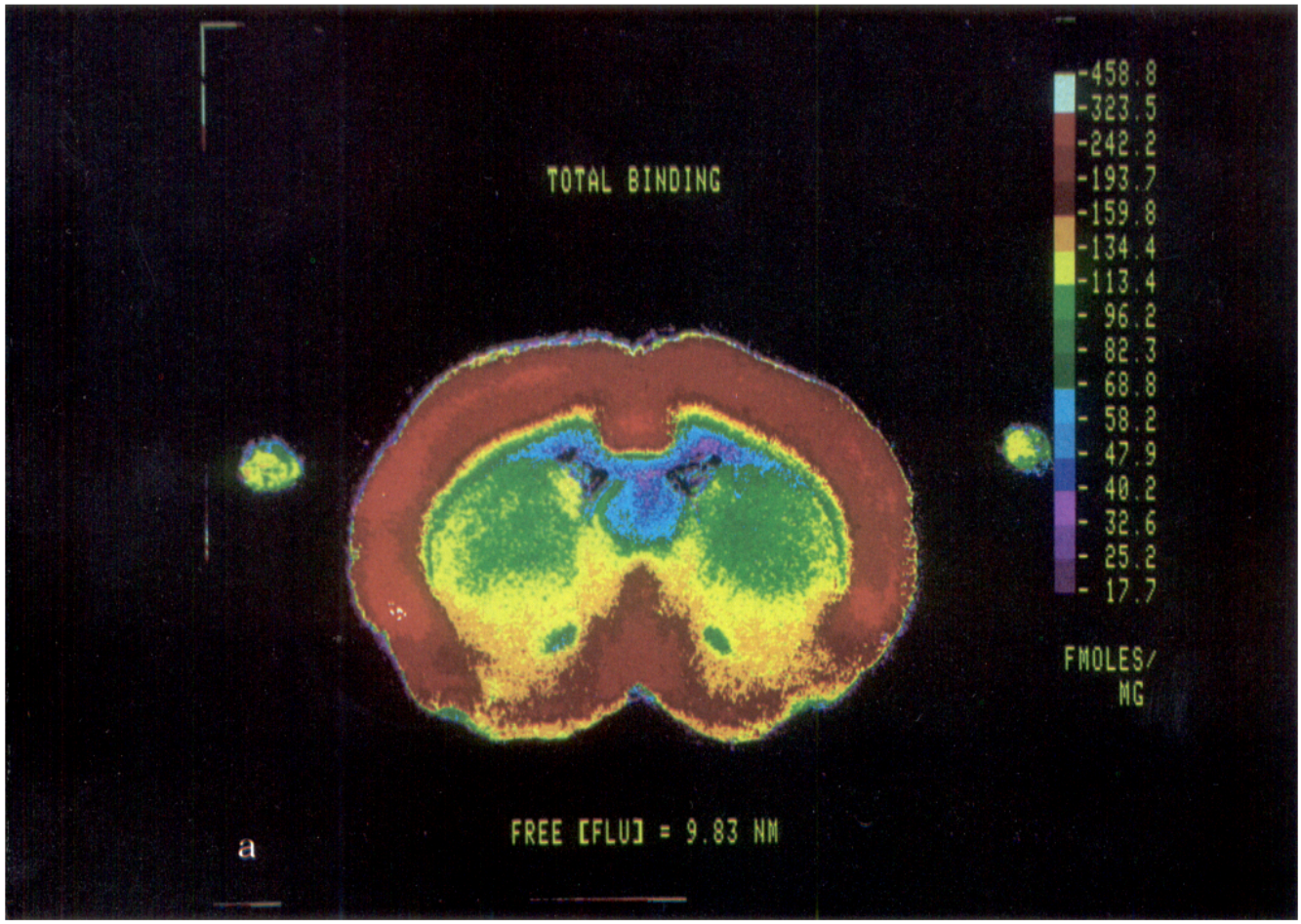
TOTAL BINDING
-458.8
-323.5
-242.2
-193.7
-159.8
-134.4
-113.4
- 96.2
- 82.3
- 68.8
- 58.2
- 47.9
- 40.2
- 32.6
- 25.2
- 17.7
FMOLES/
MG
FREE [FLU] = 9.83 NM
a

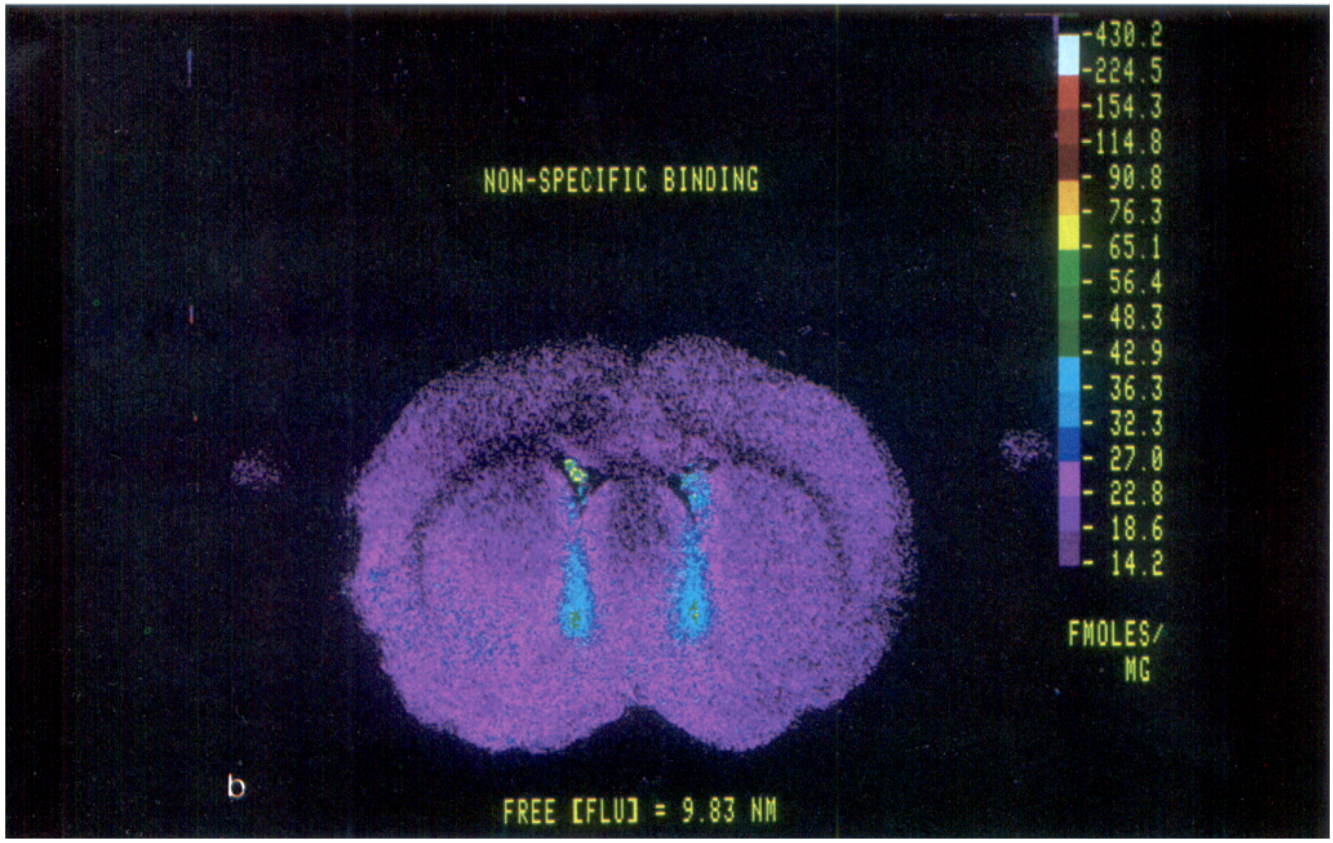
NON-SPECIFIC BINDING
-430.2
-224.5
-154.3
-114.8
- 90.8
- 76.3
- 65.1
- 56.4
- 48.3
- 42.9
- 36.3
- 32.3
- 27.0
- 22.8
- 18.6
- 14.2
FMOLES/
MG
FREE [FLU] = 9.83 NM
b

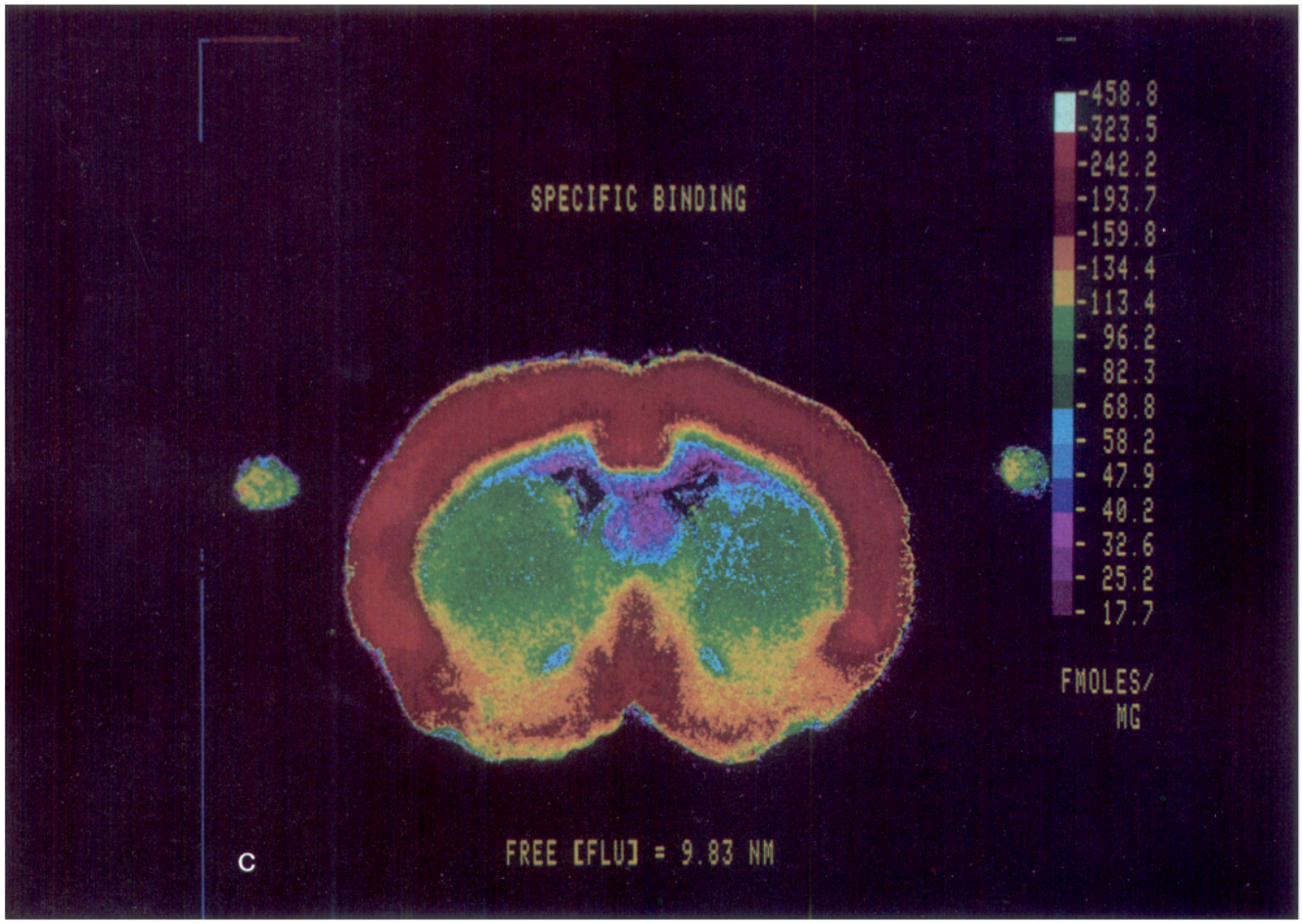

Figure 5. Pseudo-colored images of total, NSp, and specific binding of FLU (9.83 nM) generated by digitally subtracting the NSp image from the total image. Data (expressed as fmol/mg) were assigned 1 of 16 colors.

assuming that 10% of tissue weight is protein, cortical and striatal B_{max} become 2.07 and 1.02 pmol/mg protein, respectively. These values are commensurate with those cited by Pan et al. (1984).

The K_d image shown in Figure 9 is a display of the Eadie-Hofstee slopes. The average cortical pixel K_d of 0.98 nM (i.e., slope = −0.98) agrees with the K_d determined by spot densitometry. Across structures, K_d varied very little, remaining within the range of 0.83–1.08 nM. This is consistent with the findings cited for homogenates (Le Fur et al., 1979; Placeta and Karobath, 1979). These K_d values are slightly lower than those reported by others who used an autoradiographic binding protocol (Pan et al., 1984; Young and Kuhar, 1979). GABA has been shown to increase the affinity of benzodiazepine binding without altering B_{max} (Briley and Langer, 1978; Martin and Candy, 1978; Tallman et al., 1978; Unnerstall et al., 1981; Wastek et al., 1978). Since unwashed sections were used, it is likely that a significant amount of endogenous GABA was included in the incubation, resulting in a lower K_d.

Conclusion

In studies of receptor plasticity, if a binding change is found, the final question is always whether this change is due to an alteration in the total number of receptors and/or a change in their affinity. For benzodiazepine receptors, regional alterations in B_{max} have been observed following repeated seizures (Burnham et al., 1983; Kraus et al., 1983; Valdes et al., 1982), after striatal lesions (Pan et al., 1984), and in postmortem brain tissue from a patient with Huntington's disease (Penney and Young, 1982). Finally, as already discussed, benzodiazepine receptor affinities have been shown to be influenced by the presence or absence of GABA.

This paper demonstrates a technique for visualizing these 2 important binding parameters. Of the 2, the visualization of K_d is probably the more important. Visual survey of specific binding at near saturating ligand concentration can approximate what is observed from a B_{max} image, but only this pixel-by-pixel analysis can illustrate the relationship between K_d and anatomy. K_d visualization would be very useful in studying the ability of GABA to enhance benzodiazepine binding. First, the detection of regional differences in the ability of GABA to enhance affinity would be facilitated. Furthermore, areas of greatest affinity alteration could be visually compared to the distribution of GABA receptors.

This successful application of digital image technology has broad implications for the way other types of *in vitro* tissue section experiments might be analyzed. Examples of parameters that theoretically could be visualized from a pixel-by-pixel mathematical analysis are (1) individual B_{max} values for multiple classes of binding sites calculated by iterative analyses of nonlinear Eadie-Hofstee plots, and (2) IC_{50} values derived from displacement studies and based on the linear regression of a logit versus log comparison. This approach holds great promise for making a whole host of quantitative parameters calculated from autoradiographic or histochemical data amenable to visual survey and rapid quantification.

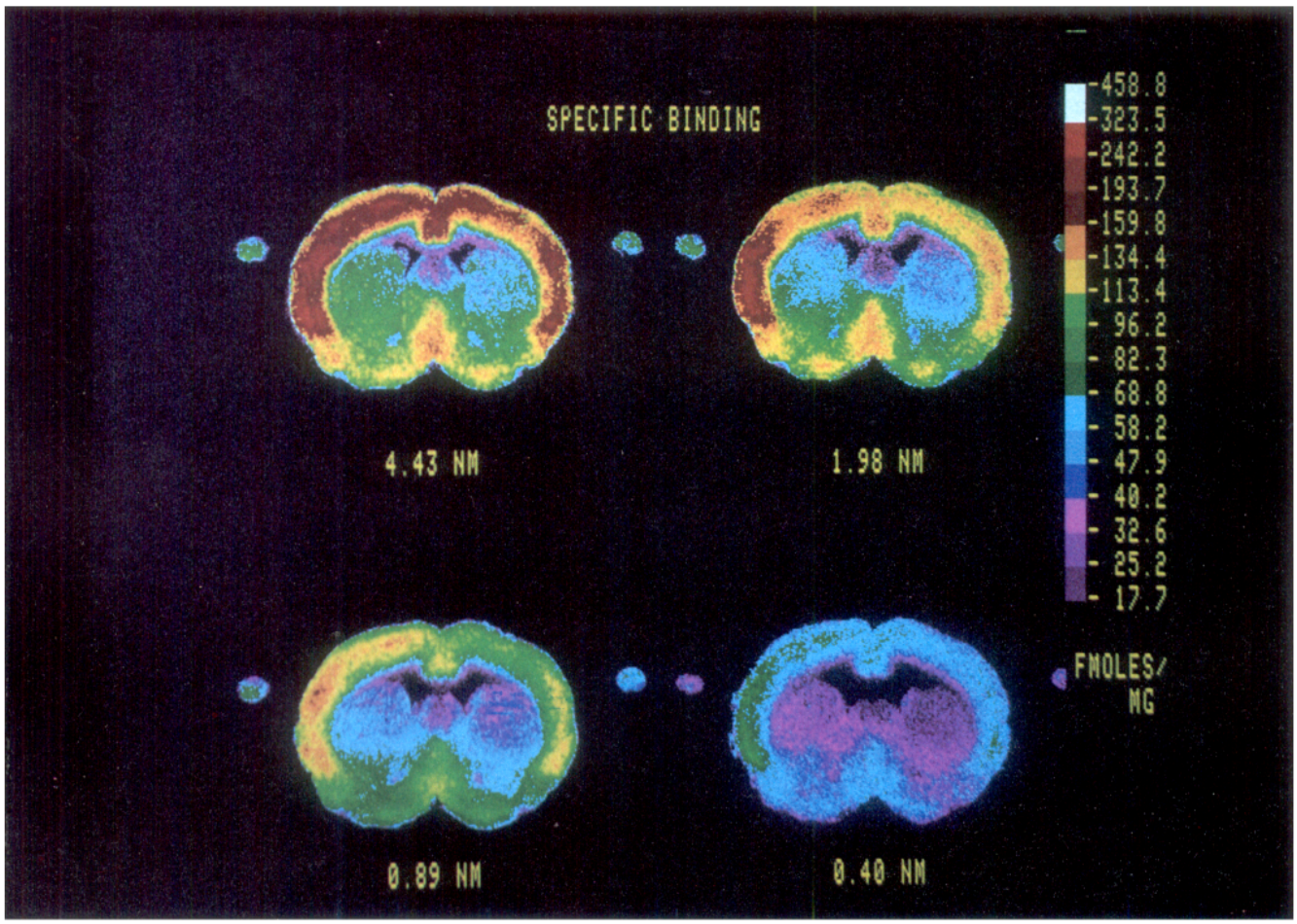

Figure 6. Specific binding images derived from incubation in the lower 4 FLU concentrations, 4.43, 1.98, 0.89, and 0.40 nM, respectively.

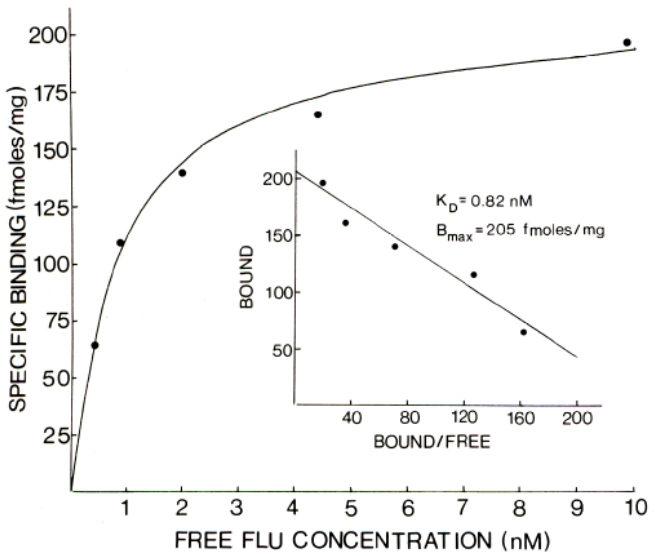

Figure 7. Saturation curve and Eadie-Hofstee plot generated from discrete measurements made in sensorimotor cortex. The values presented graphically for K_d and B_{max} are equivalent to those given in the pseudo-colored and scaled digital images. The graphical and digital image analyses were performed on the same set of autoradiograms.

Figure 8. Digital image illustrating the regional differences in B_{max}. The data have been pseudo-colored and are expressed as fmol/mg. The calculation of this image required aligning the images from a saturation study, calculating specific binding, and performing a linear regression on the images obtained from the 5 ligand concentrations.

Figure 9. Digital image illustrating the regional differences in K_d. Data expressed as nanomolar concentrations.

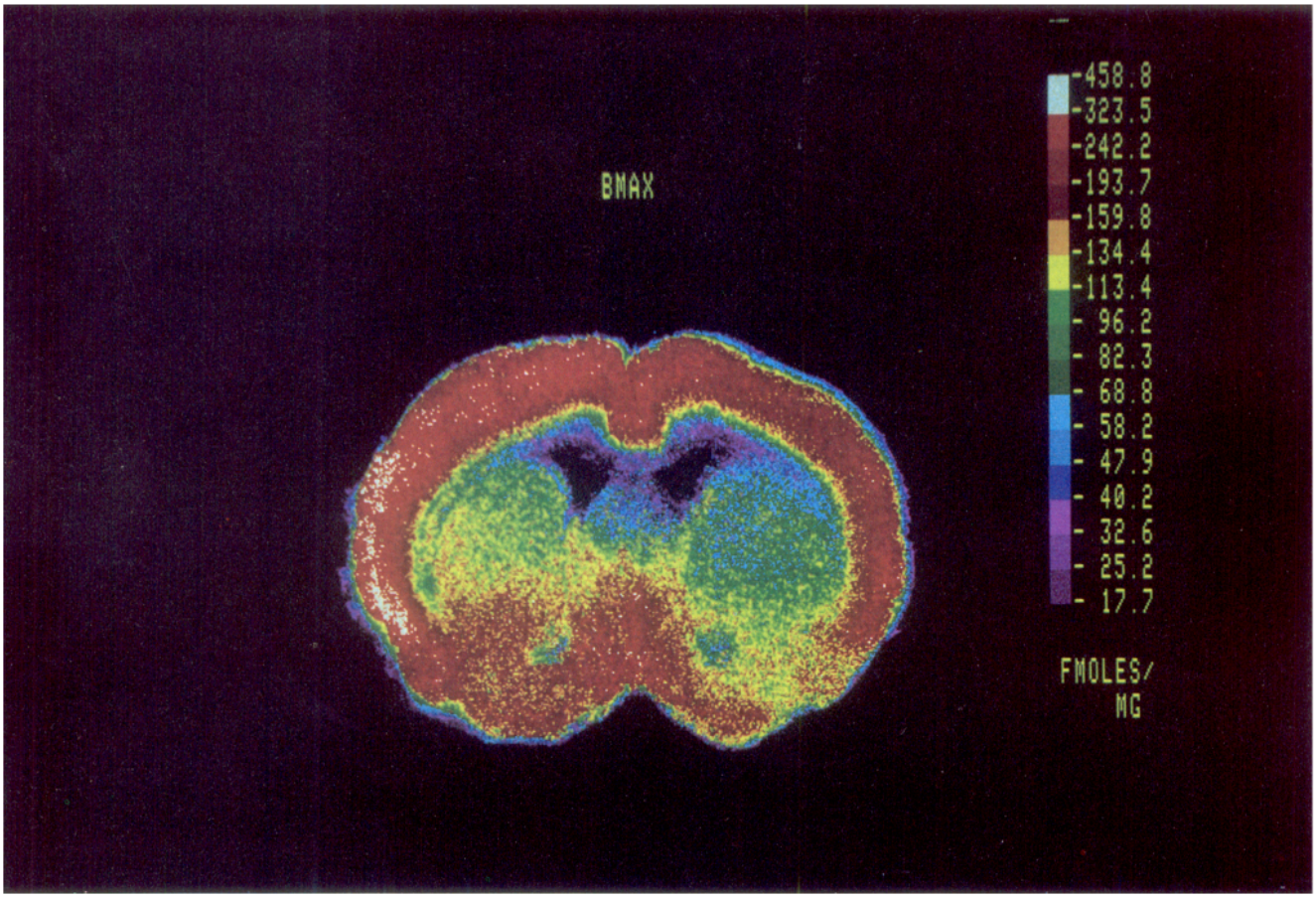
BMAX
-458.8
-323.5
-242.2
-193.7
-159.8
-134.4
-113.4
- 96.2
- 82.3
- 68.8
- 58.2
- 47.9
- 40.2
- 32.6
- 25.2
- 17.7
FMOLES/
MG

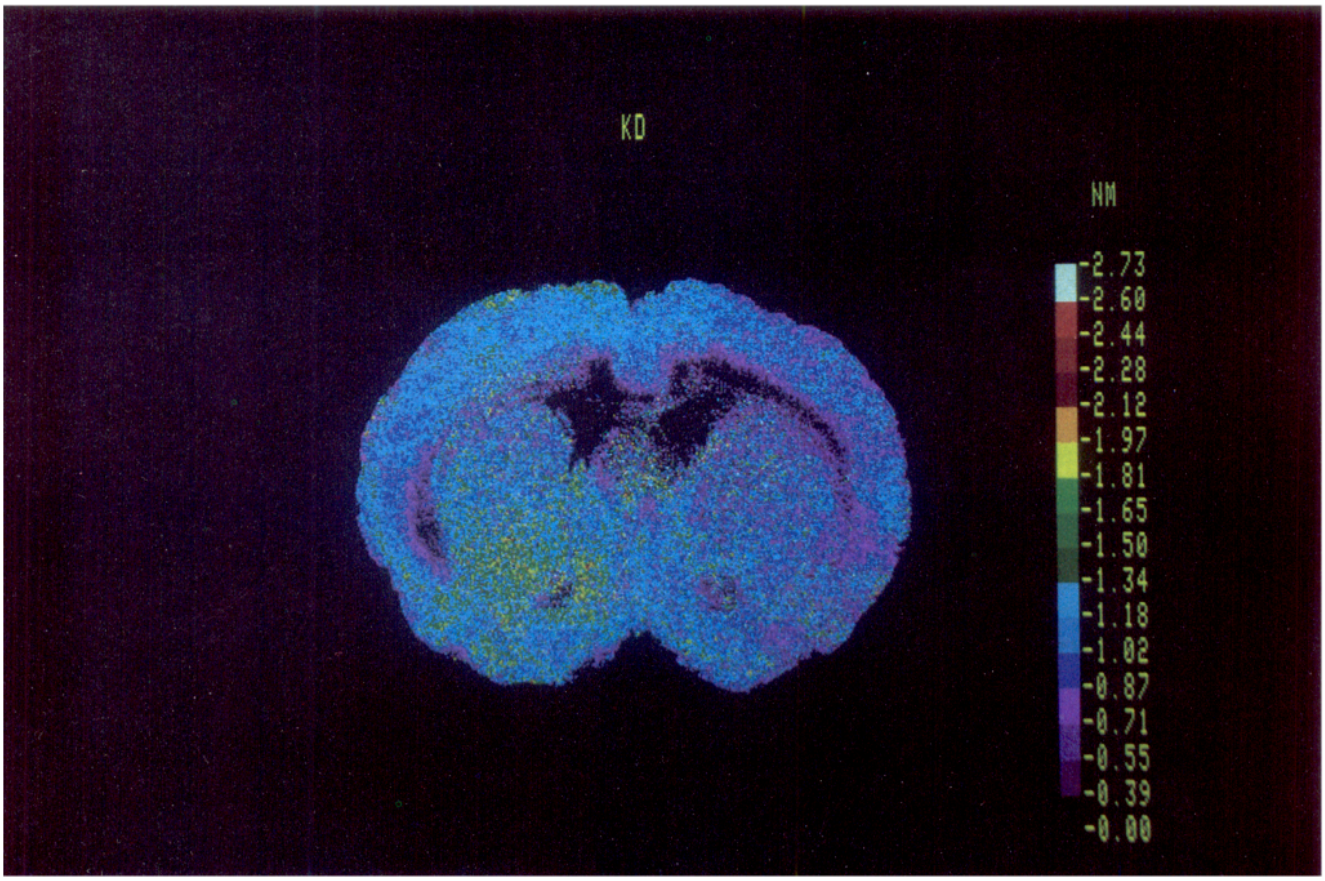
KD
NM
-2.73
-2.60
-2.44
-2.28
-2.12
-1.97
-1.81
-1.65
-1.50
-1.34
-1.18
-1.02
-0.87
-0.71
-0.55
-0.39
-0.00

References

Bosmann, H. B., K. R. Case, and P. DiStefano (1977) Diazepam receptor characterization: Specific binding of a benzodiazepine to macromolecules in various areas of rat brain. FEBS Lett. *82:* 368–372.

Braestrup, C., and R. F. Squires (1977) Specific benzodiazepine receptors in rat brain characterized by high affinity ^{3}H-diazepam binding. Proc. Natl. Acad. Sci. USA *74:* 3805–3809.

Braestrup, C., and R. F. Squires (1978) Pharmacological characterization of benzodiazepine receptors in the brain. Eur. J. Pharmacol. *48:* 263–270.

Briley, M. S., and S. Z. Langer (1978) Influence of GABA receptor agonists and antagonists on the binding of ^{3}H-diazepine to the benzodiazepine receptor. Eur. J. Pharmacol. *52:* 129–132.

Burnham, W. M., H. B. Niznik, M. M. Okazaki, and S. J. Kish (1983) Binding of [^{3}H]flunitrazepam and [^{3}H]Ro5-4864 to crude homogenates of amygdala-kindled rat brain: Two months post-seizure. Brain Res. *279:* 359–362.

Cuatrecasas, P. (1974) Membrane receptors. Annu. Rev. Biochem. *43:* 169–214.

Geary, W. A., A. W. Toga, and G. F. Wooten (1985) Quantitative film autoradiography for tritium: Methodological consideration. Brain Res. *337:* 99–108.

Goochee, C., W. Rasband, and L. Sokoloff (1980) Computerized densitometry and color coding of [^{14}C]deoxyglucose autoradiographs. Ann. Neurol. *7:* 359–370.

Kraus, V. M. B., R. M. Dasheiff, R. J. Fanelli, and J. O. McNamara (1983) Benzodiazepine receptor declines in hippocampal formation following limbic seizures. Brain Res. *277:* 305–309.

Le Fur, G., F. Guilloux, M. Mitrani, J. Mizoule, and A. Uzan (1979) Relationships between plasma corticosteroids and benzodiazepines in stress. J. Pharmacol. Exp. Ther. *211:* 305–308.

Lysz, T. W., A. W. Toga, and W. A. Geary II (1982) Standardization of ^{3}H-tissue images with different isotopic standards. Soc. Neurosci. Abstr. *8:* 645.

Martin, I. L., and J. M. Candy (1978) Facilitation of benzodiazepine binding by sodium chloride and GABA. Neuropharmacology *17:* 993–998.

Mohler, H., and T. Okada (1977) Benzodiazepine receptors: Demonstration in the central nervous system. Science *198:* 849–851.

Palacios, J. M., D. L. Niehoff, and M. J. Kuhar (1981) Receptor autoradiography with ^{3}H-sensitive film: Potential for computerized densitometry. Neurosci. Lett. *25:* 101–106.

Pan, H. S., J. B. Penney, and A. B. Young (1984) Characterization of benzodiazepine receptor changes in substantia nigra, globus pallidus and entopenduncular nucleus after striatal lesions. J. Pharmacol. Exp. Ther. *230:* 768–775.

Penney, J. B., and A. B. Young (1982) Quantitative autoradiography of neurotransmitter receptors in Huntington disease. Neurology *32:* 1391–1395.

Placeta, P., and M. Karobath (1979) Regional distribution of Na^+-independent GABA and benzodiazepine binding in sites in rat CNS. Brain Res. *178:* 580–583.

Richards, J. G., H. Mohler, and W. Haefely (1981) Benzodiazepine receptors or acceptors? Trends Pharmacol. Sci. *3:* 233–235.

Skolnick, P., and S. M. Paul (1982) Benzodiazepine receptors in the central nervous system. Int. Rev. Neurobiol. *23:* 103–140.

Squires, R. F., and C. Braestrup (1977) Benzodiazepine receptors in rat brain. Nature *266:* 732–734.

Tallman, J. F., J. W. Thomas, and D. W. Lallager (1978) GABAergic modulation of benzodiazepine binding site sensitivity. Nature *274:* 383–385.

Toga, A. W., and T. L. Arnicar (1985) Image analysis of brain physiology. Comput. Graph. Appl. *5:* 20–25.

Toga, A. W., R. L. Goo, R. Murphy, and R. C. Collins (1984) Neuroscience application of interactive image analysis. Opt. Engin. *23:* 279–282.

Toga, A. W., E. M. Santori, and R. C. Collins (1985) Visualizing K_d and B_{max}: Flunitrazepam binding parameters. Neurosci. Abstr. *11:* 1056.

Unnerstall, J. R., M. J. Kuhar, D. L. Niehoff, and J. M. Palacios (1981) Benzodiazepine receptors are coupled to a subpopulation of γ-aminobutyric acid (GABA) receptors: Evidence from a quantitative autoradiographic study. J. Pharmacol. Exp. Ther. *218:* 797–804.

Unnerstall, J. R., D. L. Niehoff, M. J. Kuhar, and J. M. Palacios (1982) Quantitative receptor autoradiography using [^{3}H]Ultrofilm: Application to multiple benzodiazepine receptors. J. Neurosci. Methods *6:* 59–73.

Valdes, F., R. M. Dasheiff, F. Birmingham, K. A. Crutcher, and J. O. McNamara (1982) Benzodiazepine receptor increases after repeated seizures: Evidence for localization to dentate granule cells. Proc. Natl. Acad. Sci. USA *79:* 193–197.

Wastek, G. J., R. C. Speth, T. D. Reisine, and H. I. Yamamura (1978) The effect of γ-aminobutyric acid on ^{3}H-flunitrazepam binding in rat brain. Eur. J. Pharmacol. *50:* 445–447.

Young, W. S., and M. J. Kuhar (1979) Autoradiographic localization of benzodiazepine receptors in the brains of humans and animals. Nature *280:* 393–395.

Young, W. S., and M. J. Kuhar (1980) Radiohistochemical localization of benzodiazepine receptors in rat brain. J. Pharmacol. Exp. Ther. *212:* 337–346.

Young, W. S., D. Niehoff, M. J. Kuhar, B. Beer, and A. S. Lippa (1981) Multiple benzodiazepine receptor localization by light microscopic radiohistochemistry. J. Pharmacol. Exp. Ther. *216:* 425–430.